

RESEARCH

Open Access



Propionic acid/FBP1 is involved in polystyrene nanoplastic-induced cardiac injury via the gut-heart axis

Huiwen Kang^{1†}, Danyang Huang^{1†}, Wei Zhang¹, JingYu Wang¹, Ziyang Liu¹, Ziyang Wang¹, Guangyu Jiang¹ and Ai Gao^{1,2*}

Abstract

Background Micro-/nanoplastics (MNPLs) are widely found in the environment and have toxic effects on various organs and systems. However, the role of the gut-cardiac axis in cardiotoxicity induced by MNPLs has not yet been elucidated through research.

Results In this study, we examined the effects of 80 nm polystyrene nanoplastics (PS-NPs) on the heart and human cardiomyocytes (AC16) cells. Histopathological examination showed that NPs caused impaired cardiac function and increased myocardial collagen deposition. In view of the potential influence of gut microbiota and its metabolites on cardiac function, we conduct this study to investigate the specific effects they have on cardiac function. Analysis of cecal contents by 16 s ribosomal RNA (rRNA) and short chain fatty acids (SCFAs) revealed that colonic tissue damage, intestinal flora disorder, and reduction of propionic acid induced by PS-MPs were closely related to cardiac function. Further transcriptomic analysis of heart and colon tissues indicated that propionic acid may reduce cardiac function by reducing the expression of fructose-1, 6-biphosphatase 1 (FBP1). The hypothesis was further verified by in vitro intervention experiments with sodium propionate and FBP1 activator (BML-275).

Conclusions In summary, our study systematically demonstrated the role of gut-heart axis in NPs-induced cardiac injury, and the specific process was that NPs exposure reduced propionate level, which in turn inhibited FBP1 expression to impair cardiac function. These findings provide new insights into NPs-induced cardiotoxicity and identify potential therapeutic targets, providing clues for the prevention and treatment of NPs-induced cardiac injury in the future.

Keywords Nanoplastics, Cardiotoxicity, Gut-heart axis, Short-chain fatty acid

[†]Huiwen Kang and Danyang Huang contributed equally to this work.

*Correspondence:

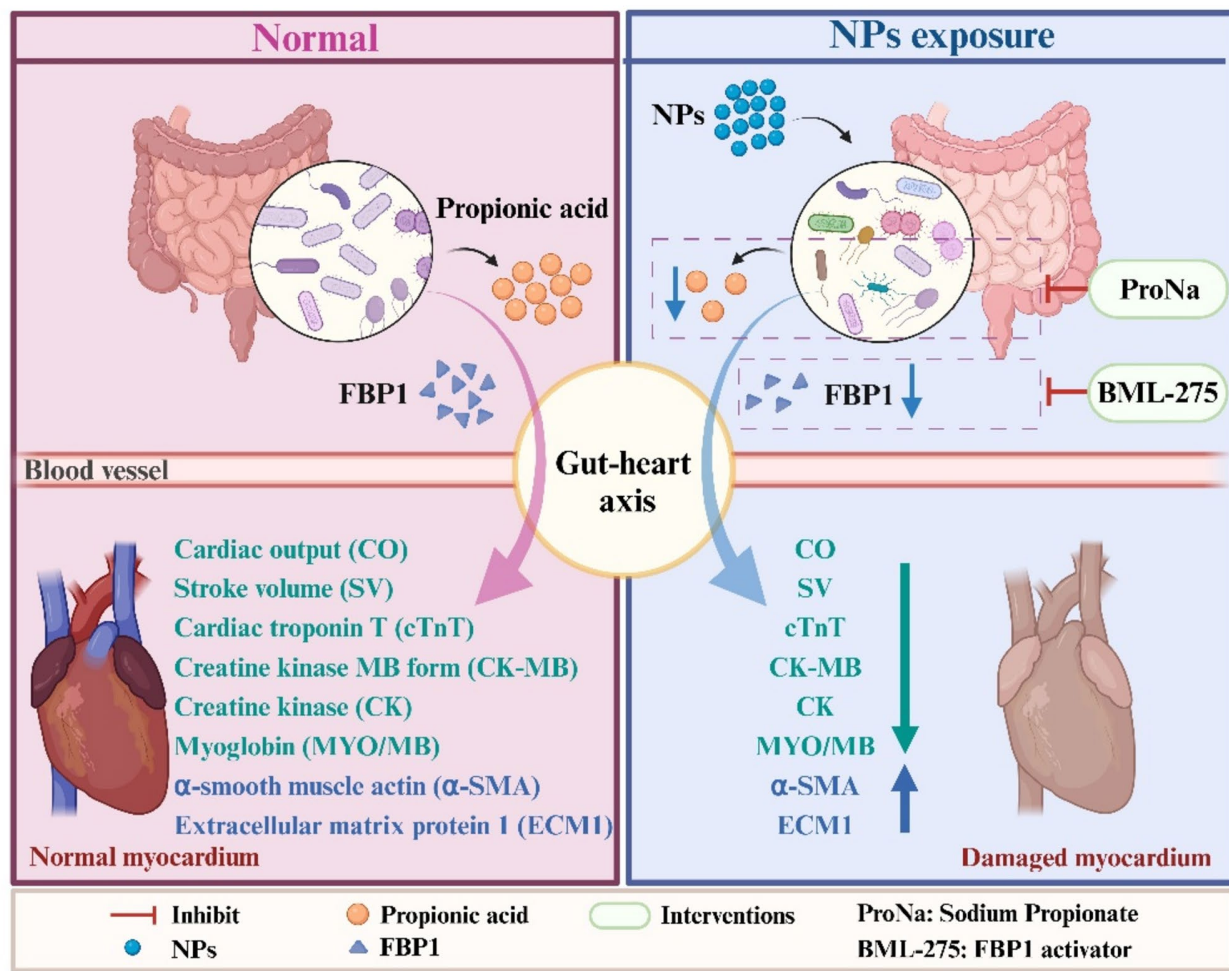
Ai Gao

gaoai428@ccmu.edu.cn

Full list of author information is available at the end of the article



Graphical Abstract



Background

Over the past few decades, plastic products have become ubiquitous due to their low cost, durability, and versatility. However, these advantages have led to significant challenges in managing plastic waste. Of particular concern are Micro-/nanoplastics (MNPLs), which are persistent in the environment and contribute to widespread ecological contamination. MNPLs have been discovered in diverse environments, from the polar ice caps [1] to the deep sea [2], as well as in freshwater systems [3], soil [4], and the air [5]. The human body is exposed to MNPLs through a variety of ways. A growing number of studies have found MNPLs in human nasal passages [6] and lung tissue [7, 8]. Research on the hazards of inhaled MPs is still limited and requires urgent attention.

A growing body of epidemiologic and experimental evidence suggests that air pollutants are strongly associated with the incidence and progression of cardiovascular disease [9], such as airborne particulate matter (PM)

and nitrogen oxides [10]. Importantly, the researchers detected MNPLs in the human heart and its surrounding tissues [11], thrombi [12], bone marrow [13], and carotid artery plaque [14], raising concerns about potential cardiovascular health risks in humans and animals. Epidemiological evidence found that patients with detected MNPLs in carotid plaque had a higher combined risk of myocardial infarction and stroke than patients without detected MNPLs [14]. Laboratory studies have found that MNPLs can cause cardiac injury in mice [15–17], rats [18, 19], chickens [20], and zebrafish [21, 22], but the exact mechanism remains to be further investigated. The gut is the body's largest immune organ. Studies have demonstrated the intratracheal instillation of multi-walled carbon nanotubes (MWCNT) exacerbates adriamycin-induced cardiotoxicity by altering the gut microbiota [23]. Furthermore, gut microbiota has been identified as a novel therapeutic target between air pollution-induced cardiovascular and metabolic diseases [24]. Therefore, it

is essential to analyze how gut microbiota disturbance caused by MNPLs affects cardiac function.

The gut-heart axis is an emerging field of medical research that highlights the complex relationship between the gastrointestinal system and cardiovascular health. Gut microbiota is a key contributor to host health and homeostasis [25]. Recent studies have shown that gut microbiota plays a crucial role in regulating cardiac function and cardiovascular diseases. Specifically, changes in gut microbiota composition are closely related to cardiovascular diseases such as hypertension, atherosclerosis, and heart failure [26]. Specific microbial metabolites, such as short-chain fatty acids (SCFAs) [27], trimethylamine-N-oxide (TMAO) [28], and bile acids [29], can influence heart health by regulating inflammation, lipid metabolism, and endothelial function [30]. Studies have found that MNPLs can cause gut microbiota disorders [12, 31]. Long-term exposure to MNPLs resulted in reduced SCFAs production [32]. However, the specific process and key molecules of gut-heart axis in MNPLs-induced cardiotoxicity are still unclear and need to be further studied. Research in this field will provide a new perspective for the control of plastic pollution and the prevention of human diseases.

This study aimed to evaluate the potential cardiac toxicity of polystyrene nanoplastics (PS-NPs) in mammals, with a particular focus on the role of the gut-heart axis in NPs-induced cardiac injury. NPs concentrations equivalent to those in real-world environments were chosen to assess their impact on cardiac function, intestinal flora composition, and the production of SCFAs metabolized by gut microbiota. Key molecular targets were identified through transcriptomic analysis of heart and colon tissues, as well as through *in vivo* and *in vitro* experiments. The findings from this study provide novel insights and scientific evidence regarding the cardiotoxic effects of environmental NPs exposure. Additionally, the results offer potential strategies for prevention and mitigation of NPs-induced cardiac damage through modulation of gut-cardiac crosstalk.

Results

Characterization of NPs

The 80 nm PS-NPs exhibited a regular, uniform spherical morphology, as observed through scanning electron microscopy (SEM) (Fig. 1A). These findings suggest that the NPs possess good stability and dispersion. The zeta potential of the NPs was measured to be -33.30 ± 0.79 mV (Fig. 1B), while their hydrodynamic size was determined to be 83.54 ± 0.72 nm (Fig. 1C).

NPs reduced heart function in mice

The method of respiratory exposure to PS-NPs used in this study is illustrated in Fig. 1D. The NPs group showed

no significant changes in body weight compared with the control group (Fig. S1A). Additionally, the organ coefficients for the heart decreased in a dose-dependent manner (Fig. S1B). Echocardiography was employed to assess the anatomical structure and functional status of the heart and major vessels, thereby reflecting overall heart function. PS-NPs exposure resulted in reduced CO and SV, which indicates that the cardiac function of the mice was impaired (Fig. 1E and F). These findings collectively highlight the adverse effects of PS-NPs on heart performance. Exposure to NPs resulted in an incremental increase in the markers of myocardial injury cardiac troponin T (cTnT), creatine kinase MB form (CK-MB), creatine kinase (CK), and Myoglobin (MYO/MB) at all three dose groups (Fig. 1G). Electron microscopy was used to visualize the location of NPs and cardiac ultrastructure (Fig. 1H). The control myocardial tissue was structurally normal, and the mitochondria were normally distributed, uniformly arranged, and dense. After treatment with 3 mg/kg NPs, local myocardial fibers were broken and missing, and the mitochondria were obviously swollen and vacuolated. The pathologic changes in cardiac structure were further evaluated using HE staining and Masson staining (Fig. 1I). The myocardial tissue of the control group was well arranged and dense. Exposure to NPs exhibited myocardial clefts and fiber breaks, and such changes were more pronounced with increasing doses of NPs. Masson staining suggested that exposure to NPs could lead to an increased deposition of collagen fibers. The levels of the fibrosis markers α -smooth muscle actin (α -SMA) and extracellular matrix protein 1 (ECM1) both increased with dose (Fig. 1J).

NPs can cause colon injury, gut microbiota disorder, and SCFAs reduction in mice

Gut microbiome and its metabolites are closely related to a variety of cardiovascular diseases [33]. We further investigated the effects of 3 mg/kg NPs on mouse colon and gut microbiota, as well as SCFAs. Histopathological examination of colon tissue was performed using hematoxylin and eosin (H&E) and alcian blue-periodic acid-schiff (AB-PAS) staining. After 60 d of NPs exposure, a reduction in the number of columnar and goblet cells was observed, along with loose and irregularly arranged lamina propria glands. Additionally, extensive infiltration of inflammatory cells and a decrease in mucus secretion were noted (Fig. 2A and Fig. S2). To further investigate colonic barrier damage, we employed Evans blue staining and evaluated the expression of tight junction proteins (Occludin, Claudin-1, and zonula occludens-1 (ZO-1)) to characterize intestinal permeability. Our results demonstrated that NPs exposure caused significant colonic barrier damage (Fig. 2B), accompanied by a marked reduction in both gene and protein expression levels of

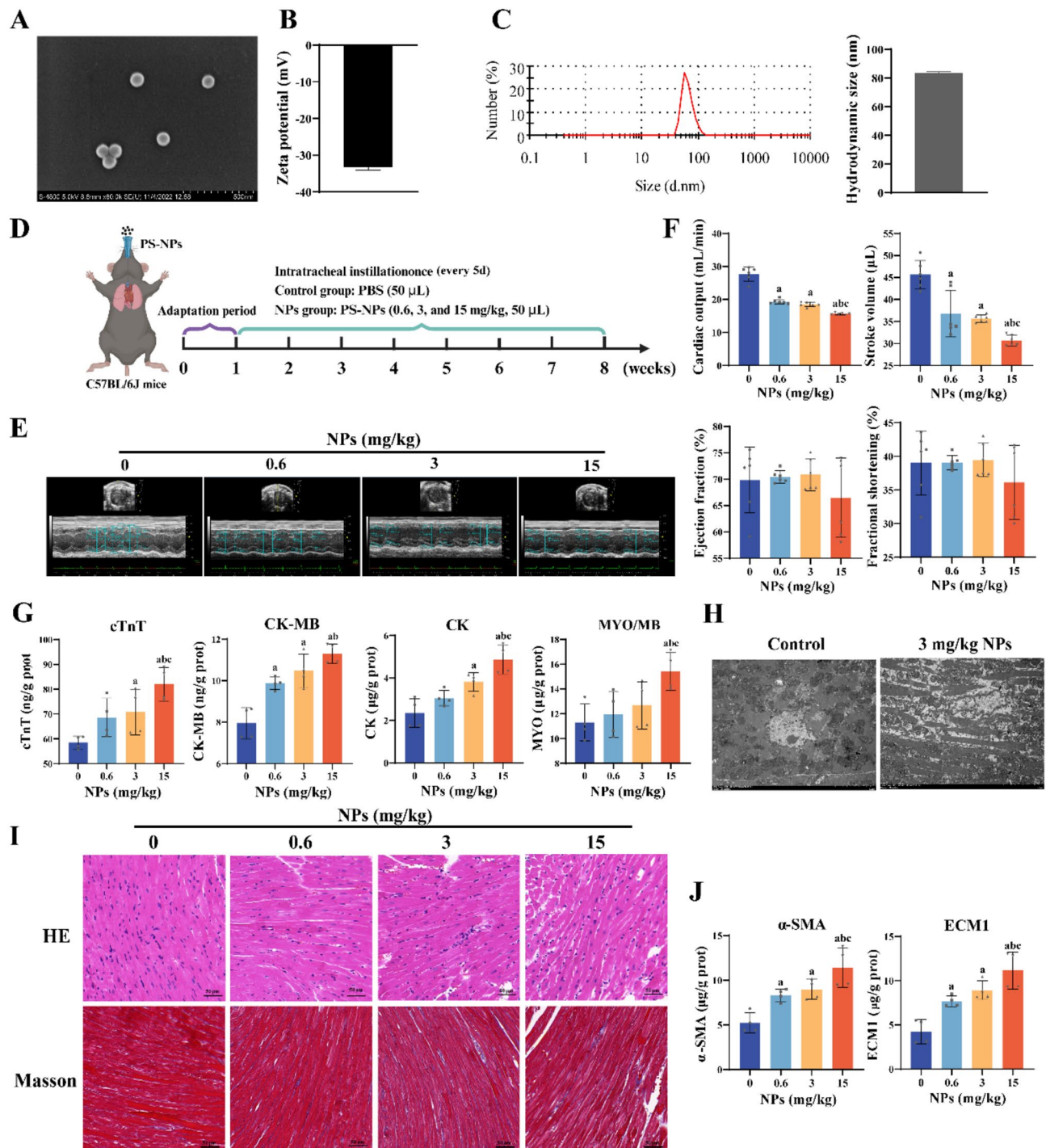


Fig. 1 Characterization of NPs and its effect on cardiac function in mice. **(A)** The image of NPs. **(B)** Zeta potentials of NPs. **(C)** The hydrodynamic size of NPs. **(D)** Schematic diagram of the experimental procedure. **(E-F)** The effects of NPs at different doses on cardiac function were examined by echocardiography. **(G)** Effect of different doses of NPs on the expression of myocardial injury markers. **(H)** Effect of NPs on cardiac ultrastructure. **(I-J)** NPs exposure to cardiac tissue damage and collagen deposition. ^a*p* < 0.05, compared with the 0 mg/kg group; ^b*p* < 0.05, compared with the 0.6 mg/kg group; ^c*p* < 0.05, compared with the 3 mg/kg group, *n* ≥ 3

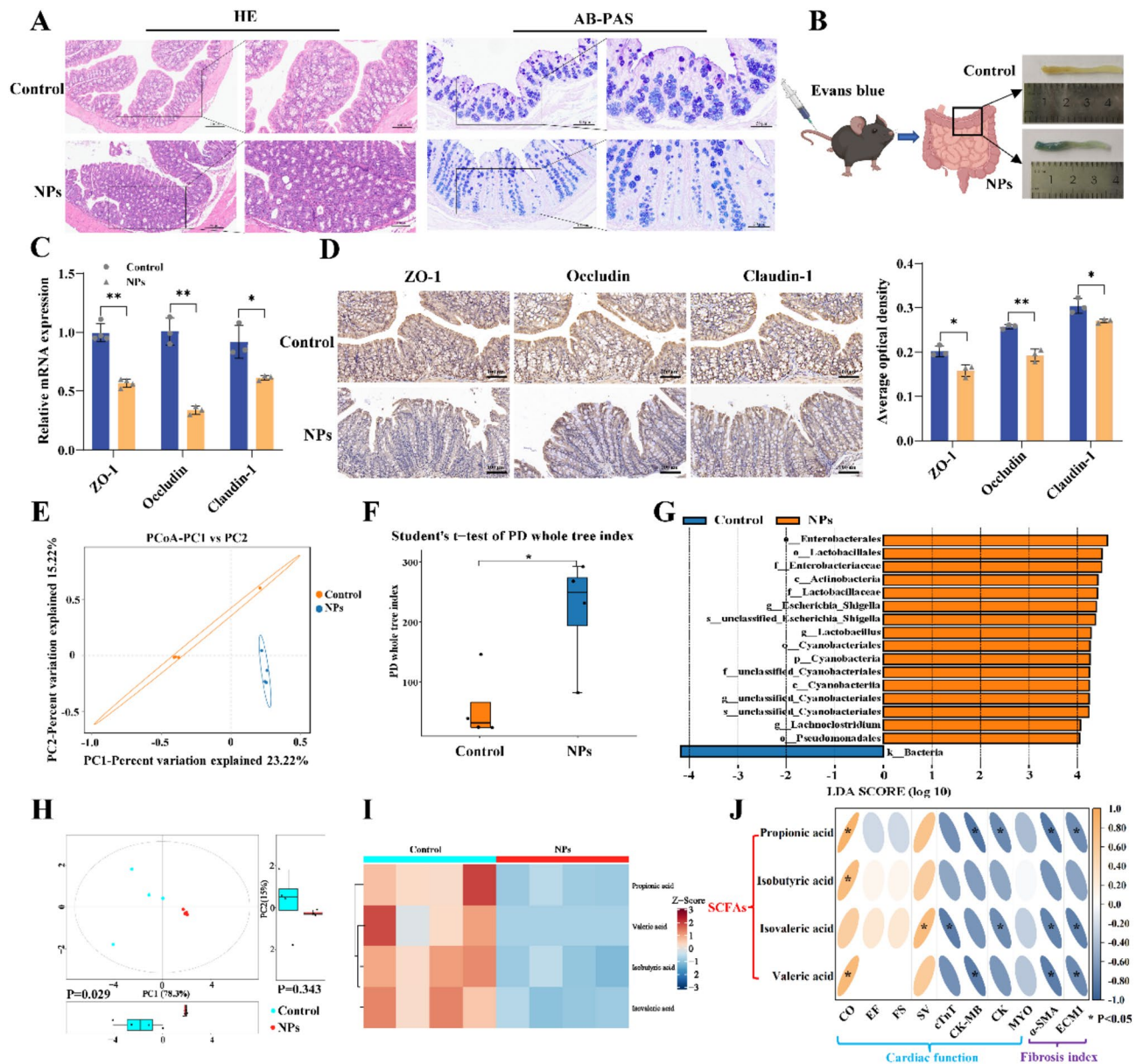


Fig. 2 NPs (3 mg/kg) led to injury of the colon, disturbance of the intestinal flora, and disorder of short-chain fatty acids (SCFAs). **(A)** Effect of NPs on colonic tissue. **(B–D)** Effect of NPs on colon barrier in mice. **(E)** PCoA score plots of intestinal flora. **(F)** Alpha diversity index results between groups. **(G)** NPs causes differences in gut microbiota. **(H)** PCA score plot with principal component boxplot of SCFAs. **(I)** Expression clustering heatmap of SCFAs. **(J)** Correlation of SCFAs with cardiac function and fibrosis index. ** $p < 0.01$, * $p < 0.05$, $n \geq 3$

Occludin, Claudin-1, and ZO-1 (Fig. 2C–D). These findings indicate that NPs exposure compromises intestinal integrity, contributing to increased gut permeability. Next, we found that NPs can cause changes in the gut microbiota of mice (Fig. 2E), including the diversity of microbiota (Fig. 2F) and species of the microbiota (Fig. 2G).

SCFAs, produced by the metabolism of intestinal microbiota, play a crucial role in various pathophysiological processes of the cardiovascular system [34]. To assess the impact of NPs exposure on SCFAs, we measured the

levels of several SCFAs in the cecal contents of mice. Our results showed that the levels of propionic acid, isobutyric acid, isovaleric acid, and valeric acid were significantly reduced following NPs exposure (Fig. 2H–I and Fig. S3). To further investigate the relationship between SCFAs and cardiac injury, we conducted a correlation analysis between the altered SCFAs and markers of cardiac injury, including cardiac function and fibrosis indexes. A strong correlation was observed, with propionic acid showing the strongest association with cardiac damage (Fig. 2J). These results suggest that NPs exposure

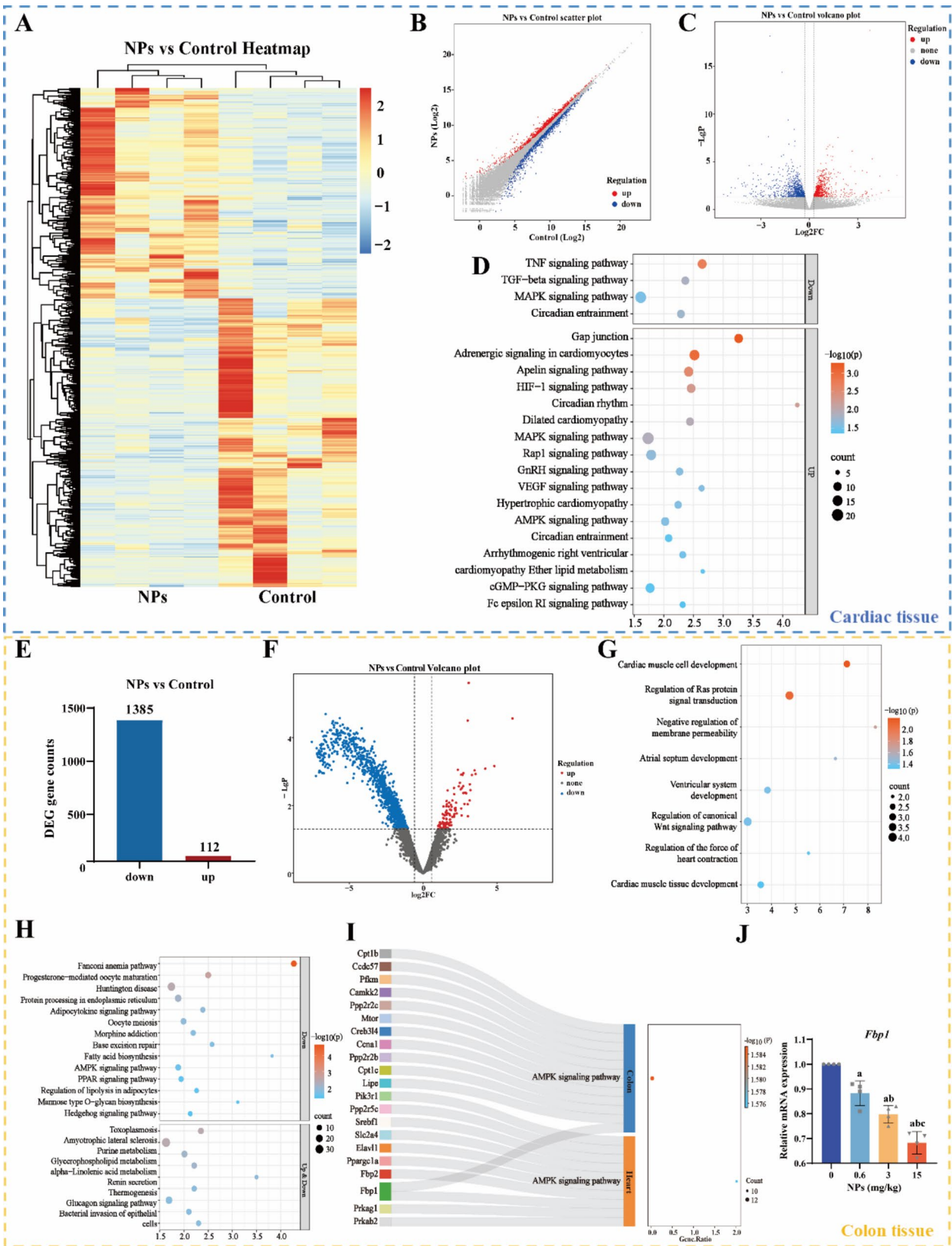


Fig. 3 (See legend on next page.)

(See figure on previous page.)

Fig. 3 Transcriptomic analysis of heart and colon revealed key molecules of cardiotoxicity in NPs. **(A-C)** Hierarchical clustering and distribution of differential genes in cardiac tissue. **(D)** Differential genes and pathways in cardiac tissue. **(E-F)** Distribution of differential genes in colon tissue. **(G)** Heart-related pathways from differential gene cluster analysis of colon tissue. **(H)** Differential genes and pathways in colon tissue. **(I)** A same pathway and its related differential genes were analyzed in heart and colon tissues. **(J)** *Fbp1* gene expression in heart tissue. ^a $p < 0.05$, compared with the 0 mg/kg group; ^b $p < 0.05$, compared with the 0.6 mg/kg group; ^c $p < 0.05$, compared with the 3 mg/kg group, $n = 4$

disrupts gut microbiota balance and SCFA production, especially propionate, which may be a key molecule in the observed cardiac dysfunction.

Fructose-1,6-bisphosphatase 1 (FBP1) is a potential key molecule in heart damage caused by NPs

In order to explore the specific mechanism of 3 mg/kg NPs induced cardiac injury, we performed transcriptomic analysis of heart tissue and colon tissue. The analysis of differentially expressed genes in the hearts of the two groups showed 17 up-regulated pathways and 4 down-regulated pathways (Fig. 3A-D). In addition, NPs induced differentially expressed genes in mouse colon tissue (Fig. 3E-F). 8 pathways related to heart were obtained by cluster analysis of colon tissue differential genes (Fig. 3G). KEGG enrichment analysis was performed on differentially expressed genes in colon tissues, and 24 signaling pathways were obtained (Fig. 3H). After comprehensive analysis of differential expression pathways in the heart and colon, we found that AMPK pathway was significantly enriched in both tissues. Notably, *Fbp1* is the only identical differential gene in both heart and colon tissue (Fig. 3I). *Fbp1* mRNA expression decreased in both colon and heart after NPs exposure (Fig. S4 and Fig. 3J). The above results suggest that FBP1 may be a molecular target for understanding the underlying mechanisms of cardiac dysfunction after NPs exposure and may provide therapeutic targets to mitigate cardiac injury.

Relationship between FBP1 and propionic acid in cardiotoxicity induced by NPs

In our study, we observed that with the increase in the dose of NPs, the expression of the FBP1 protein in heart tissue gradually declined (Fig. 4A-C). To investigate the role and potential mechanism of Propionic acid in the cardiotoxicity induced by NPs, molecular docking of FBP1 with Propionic acid was carried out. The results showed that the binding energy was -2.44 (Fig. 4D), suggesting that FBP1 might be a crucial target influencing cardiac function following the reduction of Propionic acid due to NPs exposure. Nevertheless, the specific regulatory relationship between FBP1 and propionic acid remains to be elucidated.

Propionic acid May ameliorate NPs-induced cardiac injury by regulating FBP1

In our in vitro experiments using AC16 cardiomyocytes, we evaluated heart-related indicators and the expression

of FBP1 following supplementation with sodium propionate (ProNa) (Fig. 5A). The concentrations of nanoparticles (NPs) and ProNa were selected based on cell viability assays, with optimal doses of 100 $\mu\text{g}/\text{mL}$ for NPs and 0.5 mM for ProNa (Fig. 5B-C). ProNa supplementation was found to attenuate the expression of genes associated with myocardial fibrosis induced by NPs, including tenascin C (*Tnc*), collagen type I alpha 2 chain (*Col1a2*), and actin alpha 2, smooth muscle (*Acta2*) (Fig. 5D). Furthermore, ProNa alleviated NPs-induced alterations in cardiac function-related indicators, such as MYO/MB, CK-MB, and cTnT (Fig. 5E-F). Notably, NPs significantly reduced both the mRNA and protein expression of FBP1 in AC16 cells. However, supplementation with ProNa effectively mitigated this reduction, restoring FBP1 expression levels (Fig. 5G-K). These findings suggest that propionic acid may play a protective role in counteracting NPs-induced cardiac dysfunction by modulating FBP1 expression and reducing myocardial fibrosis.

Activation of FBP1 is an effective measure to reduce heart damage caused by NPs

AMP-activated protein kinase (AMPK) plays a critical role in suppressing gluconeogenesis during energy stress, indirectly regulating the activity of FBP1 [35]. In this study, BML-275 (FBP1 activator) was used to investigate the protective role of FBP1 activation in NPs-induced cardiotoxicity (Fig. 6A). The optimal dose of BML-275, determined through cell viability assays, was found to be 10 μM (Fig. 6B). Our results revealed that BML-275 intervention effectively mitigated the NPs-induced reduction in both mRNA and protein levels of FBP1 (Fig. 6C-E). Additionally, BML-275 was able to attenuate the expression of fibrosis-related genes, including *Tnc*, *Col1a2*, and *Acta2*. Moreover, BML-275 improved the elevated levels of myocardial injury markers, such as MYO/MB, CK-MB, and cTnT (Fig. 6F-H). These results suggest that activating FBP1 expression mitigated myocardial fibrosis and cardiac dysfunction induced by NPs exposure. Therefore, FBP1 may be a potential therapeutic target to address NPs-induced cardiotoxicity.

Discussion

Plastic pollution, particularly long-term exposure to MNPLs, has emerged as a significant threat to global ecosystems and human health. Current evidence indicates that MNPLs exert toxic effects on both the heart and colon, often accompanied by disruptions in the gut

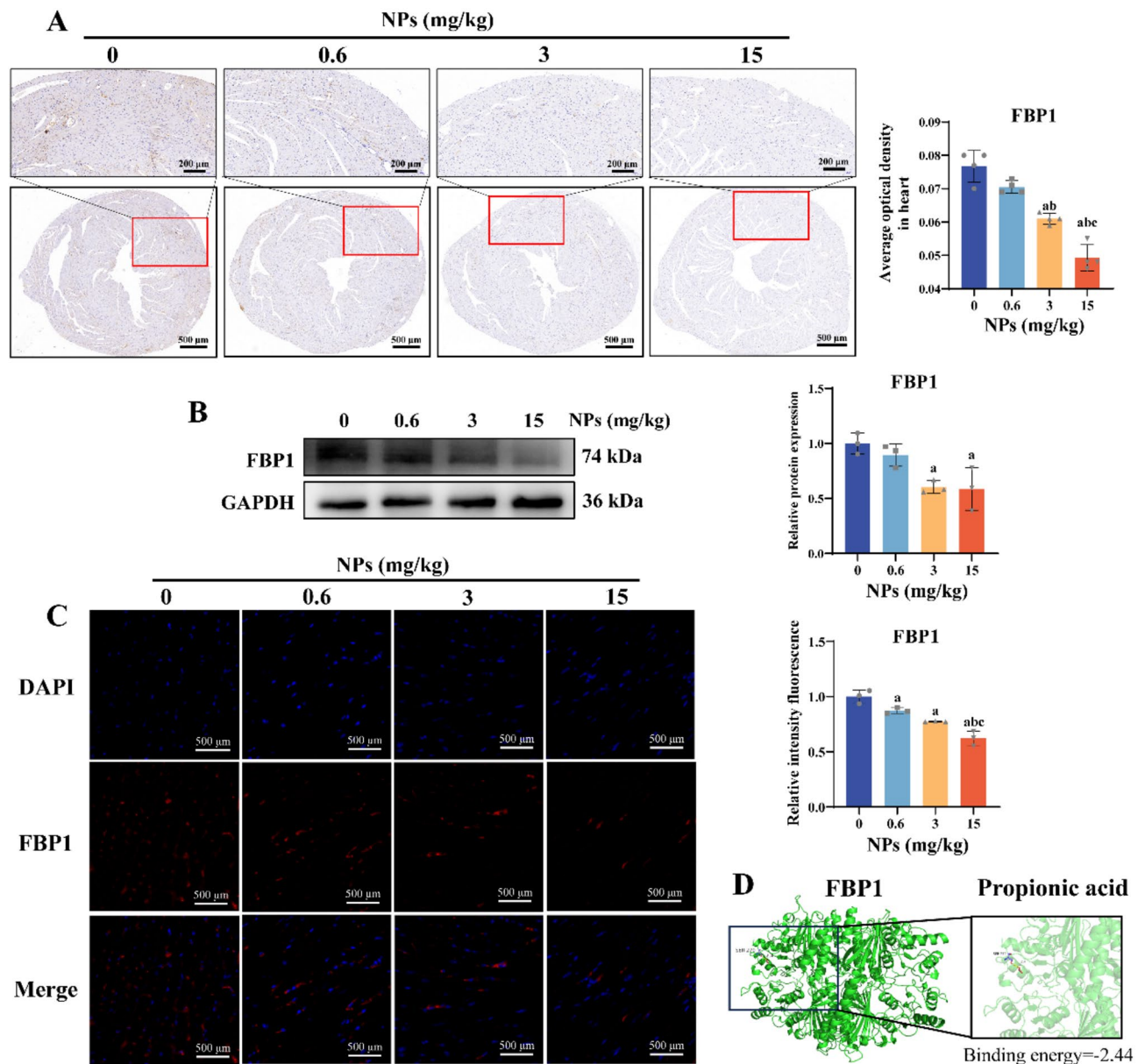


Fig. 4 Expression of FBP1 protein in cardiac tissue and its interaction with propionic acid. **(A–C)** Immunohistochemistry, western blot, and immunofluorescence were used to detect the expression of FBP1 protein. **(D)** The interaction between FBP1 protein and propionic acid. ^a $p < 0.05$, compared with the 0 mg/kg group; ^b $p < 0.05$, compared with the 0.6 mg/kg group; ^c $p < 0.05$, compared with the 3 mg/kg group, $n \geq 3$

microbiota. However, the precise role of the microbiome in MNPLs-induced cardiac injury remains poorly understood. In this study, we investigated the impact of NPs on cardiac function and explored the potential involvement of the gut-heart axis in NPs-induced cardiac injury. Furthermore, we found that NPs exposure led to gut microbiota dysbiosis and altered SCFAs profiles, indicating that disturbances in the gut microbiome may contribute to NPs-induced cardiac damage.

Age and work environment are recognized as crucial factors influencing MPs intake, as indicated in [36]. To simulate the exposure of different exposed populations,

we designed a 5-fold concentration gradient based on the calculated doses that mimic environmental exposure. Accumulating evidence showed that MNPLs can cause cardiotoxicity in experimental animals under different exposure modes. (1) Ingestion of MNPLs in the digestive tract can cause apoptosis of cardiac cells [15], damage of myocardial structure [16], and decline of cardiac systolic function [17] in mice. It can also cause the increase of myocardial enzyme level [18], myocardial structural damage and apoptosis, and myocardial collagen hyperplasia [19] in rats. It can also cause myocardial scorch death, inflammatory cell infiltration and mitochondrial

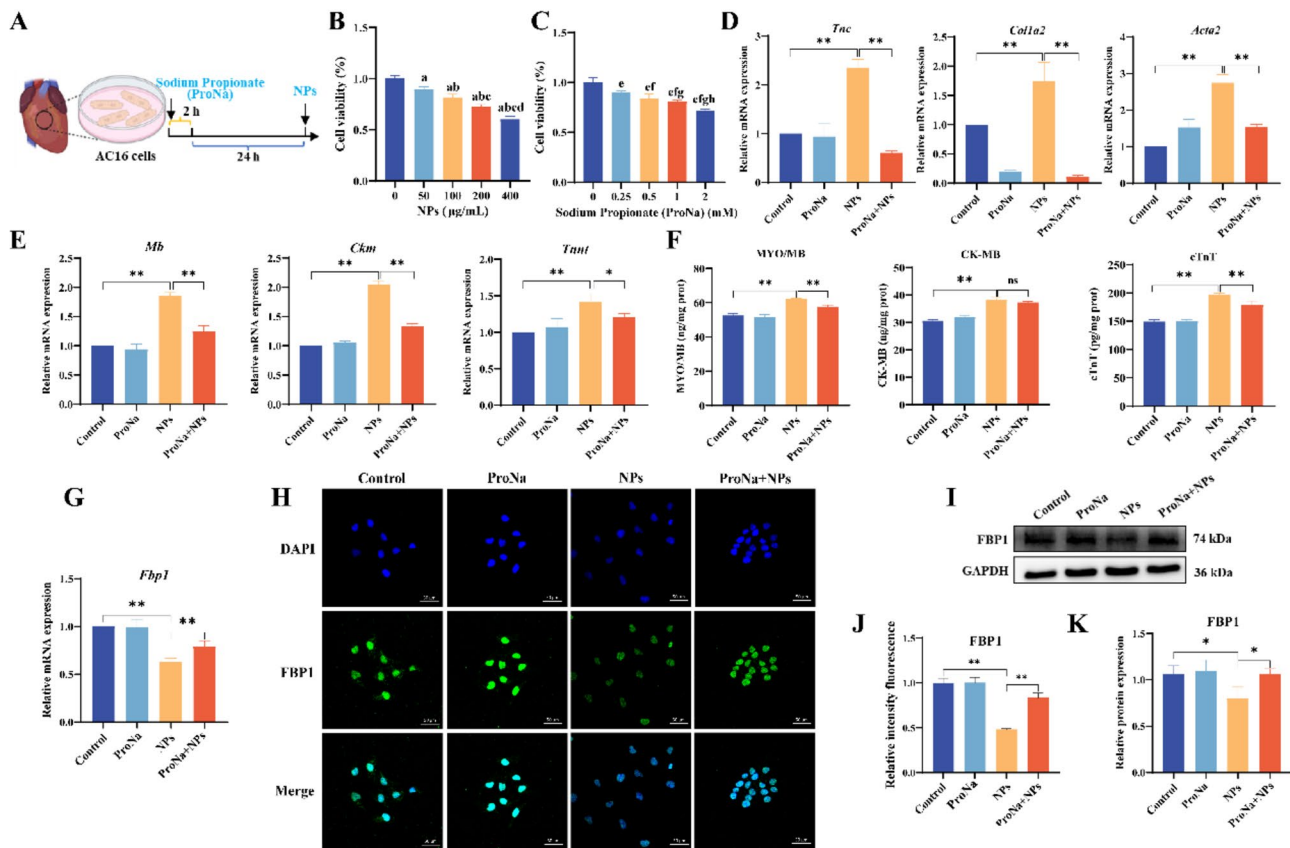


Fig. 5 Alleviating effect of Sodium propionate (ProNa) on cardiotoxicity induced by NPs. **(A)** Schematic diagram of ProNa intervention experiment. **(B)** Cell viability at different concentrations of NPs. **(C)** Cell viability at different concentrations of ProNa. **(D)** Expression of genes related to cardiac collagen deposition. **(E)** Gene expression of cardiac function related indicators. **(F)** Expression of cardiac function related indicators. **(G)** Gene expression of *Fbp1*. **(H-K)** immunofluorescence and western blot were used to detect the expression of FBP1 protein. ^a $p < 0.05$, compared with the 0 $\mu\text{g/mL}$ group; ^b $p < 0.05$, compared with the 50 $\mu\text{g/mL}$ group; ^c $p < 0.05$, compared with the 100 $\mu\text{g/mL}$ group; ^d $p < 0.05$, compared with the 200 $\mu\text{g/mL}$ group. ^e $p < 0.05$, compared with the 0 μM group; ^f $p < 0.05$, compared with the 0.25 μM group; ^g $p < 0.05$, compared with the 0.5 μM group; ^h $p < 0.05$, compared with the 1 μM group. ^{**} $p < 0.01$, ^{*} $p < 0.05$, ^{ns} $p > 0.05$, $n \geq 3$

disease in chickens [20]. Oral administration of MNPLs can cause decreased heart rate [37], pericardial edema [21, 22], and decreased cardiac function [38] in zebrafish. (2) Intraperitoneal injection of MNPLs can cause damage to myocardial structure in mice [39]. (3) Inhalation of MNPLs can cause cardiac hypertrophy in mice [40]. MNPLs may also pose a significant risk to the cardiovascular system. Notably, there are few studies on cardiotoxicity induced by respiratory ingestion of MNPLs, and the underlying mechanisms are unclear and need to be urgently addressed.

Gut microbiota participates in the maintenance of host health by producing a variety of metabolites [41]. These microbial metabolites, such as SCFAs, bile acids, and tryptophan derivatives, are essential for regulating numerous physiological processes [42]. SCFAs, for instance, are produced from the fermentation of dietary fibers and contribute to energy homeostasis, immune modulation, and the maintenance of gut barrier integrity [43]. The balance of these metabolites is crucial for

preventing inflammation, metabolic disorders, and other chronic diseases [44]. Environmental pollutants, such as heavy metals, airborne particulate matter, pesticides, and plastic particles, can significantly impact the composition of the gut microbiota [45]. These pollutants enter the body through various routes, disrupting the normal microbial balance. Studies have found that inhalation of $\text{PM}_{2.5}$ can cause gut microbiota [46] and SCFAs disorder [47], and cause cardiac toxicity [48]. Similarly, as a small particle size, NPs may also affect cardiac function through the same pathway, and the specific mechanism needs to be further studied. Our research has found that exposure to environmental doses of NPs can cause gut microbiota disturbance and decrease SCFAs, including propionic acid, isobutyric acid, isovaleric acid, and valeric acid. Through correlation analysis with cardiac function and fibrosis related indicators, we found that propionic acid was more strongly correlated with cardiac injury. Propionic acid can lower serum low density lipoprotein and total cholesterol in patients with

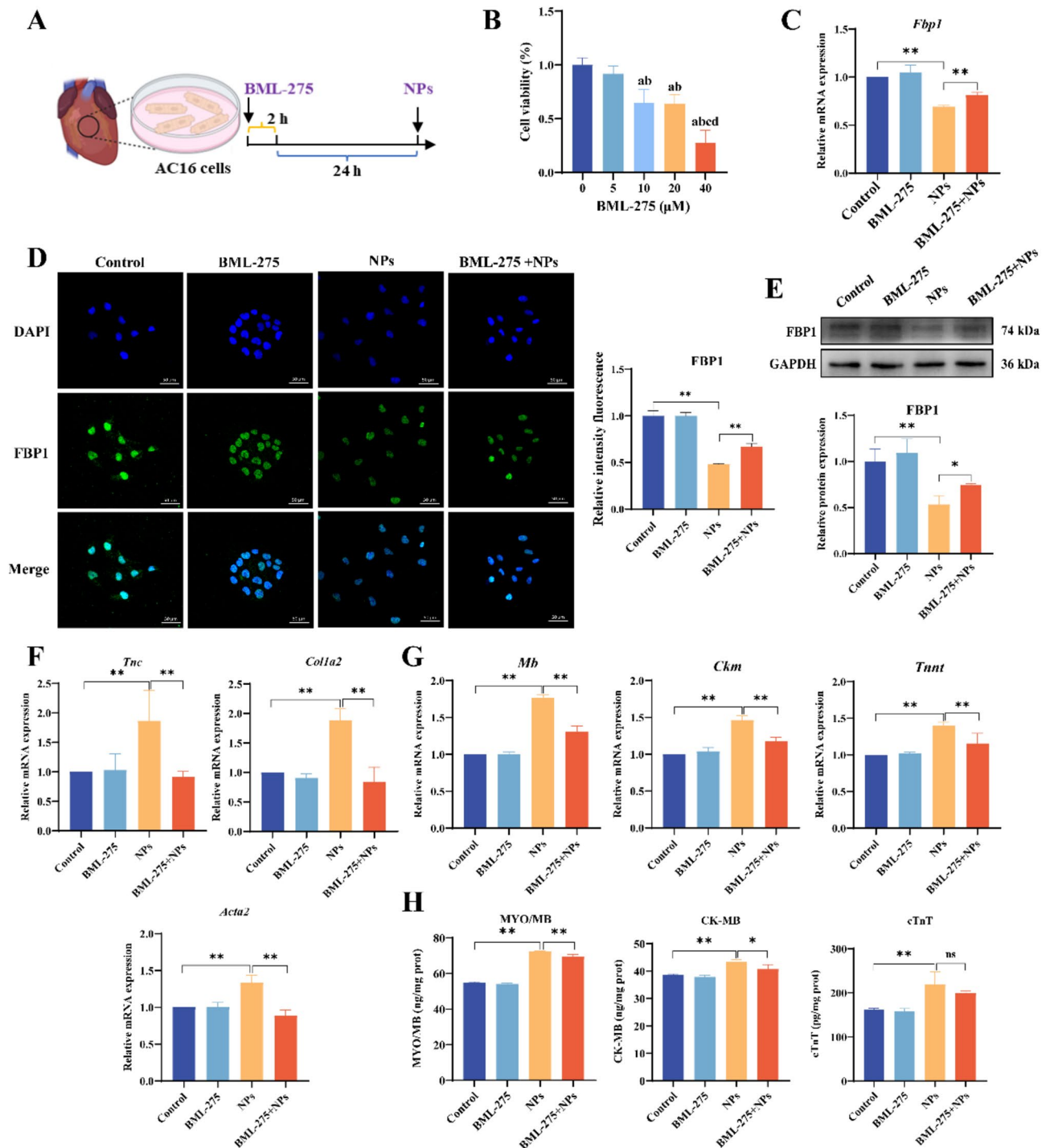


Fig. 6 Role of *Fbp1* in cardiotoxicity induced by NPs. **(A)** Schematic diagram of BML-275 intervention experiment. **(B)** Cell viability at different concentrations of BML-275. **(C)** Gene expression of *Fbp1*. **(D-E)** immunofluorescence and western blot were used to detect the expression of FBP1 protein. **(F)** Expression of genes related to cardiac collagen deposition. **(G)** Gene expression of cardiac function related indicators. **(H)** Expression of cardiac function related indicators. ^a $p < 0.05$, compared with the 0 μM group; ^b $p < 0.05$, compared with the 5 μM group; ^c $p < 0.05$, compared with the 10 μM group; ^d $p < 0.05$, compared with the 20 μM group. ^{**} $p < 0.01$, ^{*} $p < 0.05$, ^{ns} $p > 0.05$, $n \geq 3$

hypercholesterolemia [27]. An animal study found that propionate plays an important role in improving cardiovascular health by reducing atherosclerosis and hypertensive heart remodeling [49]. This study found that

NPs exposure reduced propionic acid levels in the cecal contents of mice. In conclusion, propionic acid may be involved in the process of NPs causing heart damage, but the specific process remains to be studied.

Through transcriptomic analysis of heart and colon tissue, this study identified the key pathway of NPs induced cardiac injury. One of the key findings was that FBP1 in the AMPK pathway emerged as a critical regulator of the gut-heart axis during NPs-induced heart injury. FBP1 is a pivotal enzyme in gluconeogenesis, responsible for maintaining glucose homeostasis, particularly under conditions of energy stress. AMPK plays a central role in inhibiting gluconeogenesis during energy stress, indirectly regulating FBP1 activity [35]. By modulating FBP1, AMPK ensures the proper balance between energy demand and supply in the heart. Our study demonstrated that NPs exposure alters the FBP1, contributing to cardiac dysfunction. These findings highlight FBP1 as a key molecule in understanding the molecular mechanisms of NPs-induced cardiac damage and point to the FBP1 as a potential therapeutic target for mitigating cardiovascular disease risk associated with environmental nanoparticles. Propionic acid, a SCFAs primarily produced by gut microbiota, plays a significant role in gluconeogenesis. Once absorbed by the liver, propionic acid is converted into propionyl-CoA, which is subsequently transformed into succinyl-CoA, an intermediate of the tricarboxylic acid (TCA) cycle. Succinyl-CoA then enters the gluconeogenic pathway, contributing to glucose production from non-carbohydrate substrates. It may have a positive influence on host metabolism [50]. Therefore, propionic acid may promote gluconeogenesis through the activation of FBP1, thereby helping to maintain glucose homeostasis. In our study, molecular docking analysis revealed that propionic acid directly interacts with FBP1. The supplementation of propionic acid was found to reverse the decline in FBP1 expression induced by NPs, and subsequently restored cardiac function-related markers. Furthermore, activation of FBP1 was associated with improvements in cardiac function indicators. These results suggest that propionic acid may attenuate NP-induced cardiac injury by activating FBP1, thereby highlighting a potential protective mechanism that involves the regulation of cardiac gluconeogenesis.

Conclusions

In summary, our study provides new insights into the cardiotoxic effects of NPs and underscores the importance of the gut-heart axis in mediating these effects. The results suggest that propionic acid disturbance caused by intestinal dysbiosis may be a key process in NP-induced cardiac dysfunction through increased FBP1 expression. Supplementing propionic acid or activating FBP1 *in vitro* is an effective measure to alleviate heart damage caused by NPs. Future studies should focus on further elucidating the molecular mechanisms underlying the gut-cardiac interactions in the context of NP exposure

and exploring potential strategies to restore gut microbial balance as a means of preventing cardiovascular damage.

Materials and methods

Materials and reagents

The 80 nm PS-NPs particles used in this study were purchased from the Baseline Chromatographic Technology Development Center (Tianjin, China). Firstly, the morphology of NPs was observed by scanning electron microscopy (Hitachi S-4800, Japan). The hydrodynamic size and zeta potential of NPs were further measured by Nano ZSP Expert Colloid & Protein (Malvern, UK) at 25 °C.

Animal and treatments

Six weeks old C57BL/6J male mice (Vital River Laboratory Animal Technology, China) were kept in standard specific pathogen free (SPF) environment with temperature of (22 ± 2) °C, humidity of 50-60%, light/dark cycle of 12 h for 7 days. Mice were randomly divided into four groups ($n = 8$). Subsequently, mice received intratracheal instillations of 50 µL phosphate-buffered saline (PBS) containing 0 (Control group), 0.6, 3, or 15 mg/kg (NPs group) of PS-NPs in every 5 d (specific methods of intratracheal instillations and the procedure for calculating the exposure dose are provided in the Supporting Information) [51]. The treatments were administered for 60 d, after which the mice were euthanized for further analysis. All experiments in this study were approved by the Capital Medical University Animal Care and Use Committee (AEEI-2020-168).

Cell culture and experimental design

Human cardiomyocytes (AC16) were cultured in DMEM/F12 (Gibco, USA) supplemented with 10% fetal bovine serum (Gibco, USA) and 1% penicillin-streptomycin solution (Biosharp, China). The cells were treated with 0, 50, 100, 200, and 400 µg/mL PS-NPs for 24 h. Cell cultures were performed at 37 °C in a sterilized incubator with 5% CO₂.

The optimal exposure doses of Sodium propionate (ProNa, Shanghai yuanye Bio-Technology Co., Ltd, China; 0, 0.25, 0.5, 1, and 2 mM) [52] and BML-275 (MCE, China; 0, 5, 10, 20, and 40 µM) [53] were determined based on cell viability assays. Experimental groups were established as follows: Control group, PA or BML-275 group, NPs group, and ProNa+NPs or BML-275+NPs group. In the ProNa+NPs and BML-275+NPs groups, ProNa or BML-275 was administered 2 h prior to nanoparticle exposure, and cells were subsequently exposed to NPs for 24 h. After treatment, the protein expression of the cells was observed by immunofluorescence method or the total RNA and protein were extracted from the cells of each group.

Echocardiography

Cardiac output (CO) serves as a measure of the heart's ejection function [54], while stroke volume (SV) represents the terminal event of the cardiac cycle and serves as an indicator for detecting abnormal cardiac physiological mechanisms that may lead to a state of shock [55]. Ejection fraction (EF), defined as the percentage of blood volume ejected with each cardiac cycle, is commonly used to assess cardiac performance [56]. Fractional shortening (FS) estimates the systolic function of the left ventricle and is an index for evaluating the heart's hemodynamic status. Cardiac function in mice was evaluated using echocardiography performed with the Vevo 2100 ultrasound system (FUJIFILM Visual Sonics Inc., USA), equipped with a 30 MHz phased array transducer. The following indicators of cardiac function were measured: CO, EF, SV, and FS. These parameters were calculated as the average values over five consecutive cardiac cycles. All qualitative and quantitative analyses were conducted offline using analytic software (Visual Sonics).

Histological analyses

To analyze the histopathological changes in the heart and colon after NPs exposure, we performed the same analysis as our previous study [31, 54]. Fresh heart and colon tissues from mice in each group were isolated and fixed, embedded in paraffin, made into 4 μm thick sections, and then stained with hematoxylin-eosin (H&E), Cresyl violet (Nissl), and Alcian blue-periodic acid Schiff (AB-PAS). High-resolution images were obtained by panoramic scan (3DHISTECH, Hungary). The distribution of myocardial fibers, the distribution of colon tissue cells and the expression of mucus layer were observed for histopathological evaluation.

ELISA

The levels of cTnT, CK-MB, CK, MYO/MB, α -SMA, and ECM1 in the heart of mice and cTnT, CK-MB, and MYO/MB in AC16 cells were measured by respective mouse ELISA kits (Jiangsu Jingmei Biological Technology Co., Ltd., China) according to the manufacturer's instructions.

Transmission electron microscopy

Heart tissues (1 mm^3) were fixed with 2.5% glutaraldehyde at 4 $^\circ\text{C}$. After penetrating embedding, ultrathin Sects. (60–80 nm) were made, stained (2% uranyl acetate and 2.6% lead citrate), and then observed by transmission electron microscopy (Hitachi HT7800, Japan; resolution = 1 nm, accelerating voltage = 4.0 kV) and images were collected.

RNA-seq

Total RNA was extracted from mouse heart and colon tissues using Trizol reagent, following previously described

methods [57]. The rest of the procedure was the same as in our previous experiment [31]. Briefly, mRNA was purified from total RNA using poly-T oligo-attached. Hierarchical clustering of differentially expressed mRNAs was performed (R package pheatmap, version: 1.0.12). Kyoto Encyclopedia of Genes and Genomes (KEGG) enrichment of differentially expressed genes was performed (FDR < 0.05, FC > 1.2), and the significance was set at $p < 0.05$.

SCFAs concentrations

In this experiment, seven types of SCFAs were accurately measured and dissolved in ethyl ether (purity $\geq 99.7\%$, supplied by China National Pharmaceutical Group Corporation) to achieve a concentration of 1 mg/mL. A series of concentration - standard samples were diluted to obtain the standard curve. Thirty milligrams of cecal contents were weighed into a centrifuge tube, and 300 μL of ultra-pure water was added. The mixture was homogenized for 2 min (min). Subsequently, it was centrifuged at 4 $^\circ\text{C}$ and 18,000 g for 20 min. Then, 200 μL of the supernatant was transferred, and 50 μL of concentrated sulfuric acid diluted with 50% water was added. After that, 200 μL of an ether solution (containing an internal standard of 5 $\mu\text{g}/\text{mL}$) was added. The mixture was vortexed for 1 min, sonicated for 1 min, and then centrifuged at 12,000 rpm at 4 $^\circ\text{C}$ for 20 min. Finally, it was allowed to stand at 4 $^\circ\text{C}$ for 10 min. The supernatant diethyl ether layer was treated with anhydrous sodium sulfate (purity $\geq 99\%$, purchased from Sigma company). Ultimately, the concentrations of SCFAs were measured on a gas chromatography-time-of-flight mass spectrometer (GC/TOFMS) platform (Pegasus HT, Leco Corp, USA).

16 s ribosomal RNA (rRNA) sequencing

The detailed protocols were mentioned in our previous study [31, 58]. Principal coordinate analysis (PCoA) and one-way analysis of variance (ANOVA) were used to evaluate the species complexity and compare the abundance and diversity of gut microbiota, respectively. Differential abundance taxa were assessed by combining linear discriminant analysis (LDA) with effect size (LEfSe).

Measurement of gut barrier permeability

Evans blue dye was utilized as a marker for assessing albumin extravasation in order to evaluate barrier function. The detailed protocols were mentioned in our previous study [59]. Briefly, a 2% Evans blue dye solution was prepared. The solution was then administered via the tail vein of the experimental mice. The injection was performed with precision to ensure an accurate dose delivery. After injection, the dye was allowed to circulate within the mouse's bloodstream for exactly 15 min. This

time interval was determined based on prior research and pilot experiments to ensure sufficient distribution of the dye to relevant tissues. Subsequently, a transcordial perfusion with PBS was initiated. The process was closely monitored, and the perfusion was continued until the effluent from the right atrium appeared completely colorless. This visual cue was used as an indication of successful clearance of the dye from the circulation, ensuring that any observed Evans blue staining in the tissues was due to extravasation rather than remaining dye in the blood vessels. Following the perfusion, the gut tissues of mice in each experimental group were carefully excised. The gut tissues of mice in each group were photographed and observed.

Immunohistochemistry

The immunohistochemistry analysis was conducted as previously described [31]. Heart tissue sections were incubated overnight at 4 °C with primary antibodies targeting Occludin, Claudin-1, ZO-1, and FBP1 at a dilution of 1:500 (Santa, USA). Following incubation with the primary antibodies, the sections were treated with horseradish peroxidase (HRP)-conjugated secondary antibodies and developed using 3,3'-diaminobenzidine (DAB) substrate (Sigma-Aldrich, USA) to visualize the staining. Images of the stained sections were captured using a panoramic scanner (3DHISTECH, Hungary).

Cell counting kit-8 (CCK-8)

The AC16 cells were seeded in 96-well culture plates (37 °C, 5% CO₂). After plating the cells for 24 h, they were treated with PS-NPs (0, 50, 100, 200, and 400 µg/mL), ProNa (0, 0.25, 0.5, 1, and 2 mM), or BML-275 (0, 5, 10, 20, and 40 µM) for 24 h and incubated at 37 °C for 2 h.

Quantitative reverse transcription polymerase chain reaction (RT-qPCR) analysis

Total RNA was isolated from heart tissue, colon tissue, and AC16 cells using Trizol reagent. Complementary DNA (cDNA) was synthesized from the extracted total RNA samples of mice utilizing a cDNA reverse transcription kit (Allmeek, China). RT-qPCR was subsequently conducted employing the 2×PerfectHS SYBR QPCR Mixture kit (Allmeek, China) on a Bio-Rad (CFX96™ optical module). The primer sequence is shown in supplementary Table S1.

Western blot

Heart tissues or AC16 cells were homogenized using a protein extraction reagent (Nanjing KeyGen Biotech, China). Equal amounts of total protein were used for the detection of FBP1 (1:1000, Santa, USA) and GAPDH (1:5000, CST, USA) through incubation with the respective primary antibodies overnight (4 °C). The membranes

were then incubated with horseradish peroxidase-conjugated secondary antibodies (1:2000, CST, USA) at 37 °C for 1 h. Protein bands were visualized using an enhanced chemiluminescence (ECL) reagent (Millipore, USA) and quantified using ImageJ software (NIH, USA).

Immunofluorescence

The expression of FBP1 in heart tissue was evaluated using immunofluorescence staining. Briefly, tissue sections were dewaxed and rehydrated, followed by blocking with 3% bovine serum albumin at 37 °C for 30 min. The sections were then incubated overnight at 4 °C with monoclonal antibodies against FBP1 (1:500, Santa, USA). To detect the primary antibodies, Dylight 488-conjugated anti-mouse secondary antibodies (1:100, Abcam, USA) were applied at room temperature for 1 h.

For AC16 cells, cell slides were placed in culture plates, and once the cells covered approximately 80% of the slide area, corresponding treatments were applied. Cells were fixed with 4% paraformaldehyde for 20 min and permeabilized using 0.5% Triton X-100. After permeabilization, the cells were blocked with 5% goat serum (Solarbio, China) for 1 h. Cells were then incubated overnight at 4 °C with FBP1 primary antibodies (1:100, Santa Cruz Biotechnology, USA). This was followed by incubation with Dylight 488-conjugated anti-mouse secondary antibodies (1:100, Abcam, USA) at room temperature for 1 h.

Nuclei were counterstained with DAPI (Beyotime, China). Imaging were also conducted using a panoramic scanner (3DHISTECH, Hungary).

Molecular Docking

The crystal structure of propionic acid was obtained from PubChem (<https://pubchem.ncbi.nlm.nih.gov/>), and the crystal structure of FBP1 was downloaded from the RCSB Protein Data Bank (<https://www.rcsb.org/>). Both structures were prepared for docking using Autodock Tools 1.5.7. The preparation process included removing ligands and water molecules, as well as adding hydrogen atoms. The prepared files were saved in pdbqt format. For molecular docking, the compounds were imported into Autodock Tools 1.5.7, where all flexible bonds were set to be rotatable by default. Docking simulations were carried out using Autodock Tools 1.5.7, and the docking results were visualized using PyMOL 2.6.

Statistical analysis

All data are presented as mean ± standard deviation (SD). The homogeneity of variances was evaluated using Bartlett's test, and the normality of the data was assessed with the Shapiro-Wilk test. For comparisons between two groups, a two-tailed unpaired Student's t-test was used. For multiple group comparisons, one-way analysis of variance (ANOVA) was conducted, followed by Tukey's

multiple comparison test with Bonferroni correction. In cases where data did not meet the normality assumption, the Games-Howell test was employed for multiple group comparisons. Spearman correlation was used to analyze the correlation between differential SCFAs and cardiac injury related indicators. All statistical analyses were performed using SPSS version 26.0, Origin 2024, or Graph-Pad Prism version 8.3.

Supplementary Information

The online version contains supplementary material available at <https://doi.org/10.1186/s12989-025-00626-9>.

Supplementary Material 1

Author contributions

HK: performed experiments, methodology, writing (original draft); DH: performed experiments, data curation, statistical analysis; WZ, JW, ZL, ZW, and GJ: performed experiments and acquisition of data; AG: conceptualization, funding acquisition, writing (review and editing). All authors reviewed the manuscript.

Funding

This study was funded by the National Natural Science Foundation of China (82073520), the Beijing Natural Science Foundation Program and Scientific Research Key Program of Beijing Municipal Commission of Education (KZ201810025032) and the Support Project of High-level Teachers in Beijing Municipal Universities in the Period of 13th Five-year Plan (CIT&TCD 20170323).

Data availability

No datasets were generated or analysed during the current study.

Declarations

Competing interests

The authors declare no competing interests.

Conflict of interest

The authors declare that they have no conflict of interest.

Author details

¹Department of Occupational Health and Environmental Health, School of Public Health, Capital Medical University, 10 Xitoutiao, You An Men, Beijing 100069, China

²Beijing Key Laboratory of Environment and Aging, Capital Medical University, Beijing 100069, China

Received: 23 December 2024 / Accepted: 21 April 2025

Published online: 09 May 2025

References

- Materić D, Kjør HA, Vallenga P, Tison JL, Röckmann T, Holzinger R. Nanoplastics measurements in Northern and Southern Polar ice. *Environ Res*. 2022;208:112741. <https://doi.org/10.1016/j.envres.2022.112741>.
- Cunningham EM, Ehlers SM, Dick JTA, Sigwart JD, Linse K, Dick JJ, et al. High abundances of microplastic pollution in Deep-Sea sediments: evidence from Antarctica and the Southern ocean. *Environ Sci Technol*. 2020;54 21:13661–71. <https://doi.org/10.1021/acs.est.0c03441>.
- Tamayo-Belda M, Pérez-Olivares AV, Pulido-Reyes G, Martín-Betancor K, González-Pleiter M, Leganés F, et al. Tracking nanoplastics in freshwater microcosms and their impacts to aquatic organisms. *J Hazard Mater*. 2023;445:130625. <https://doi.org/10.1016/j.jhazmat.2022.130625>.
- Yang L, Kang S, Wang Z, Luo X, Guo J, Gao T, et al. Microplastic characteristic in the soil across the Tibetan plateau. *Sci Total Environ*. 2022;828:154518. <https://doi.org/10.1016/j.scitotenv.2022.154518>.
- O'Brien S, Rauer C, Ribeiro F, Okoffo ED, Burrows SD, O'Brien JW, et al. There's something in the air: A review of sources, prevalence and behaviour of microplastics in the atmosphere. *Sci Total Environ*. 2023;874:162193. <https://doi.org/10.1016/j.scitotenv.2023.162193>.
- Torres-Agullo A, Karanasiou A, Lacorte S. Nasal lavage technique reveals regular inhalation exposure of microplastics, not associated from face mask use. *Environ Int*. 2023;178:108129. <https://doi.org/10.1016/j.envint.2023.108129>.
- Amato-Lourenço LF, Carvalho-Oliveira R, Júnior GR, Dos Santos Galvão L, Ando RA, Mauad T. Presence of airborne microplastics in human lung tissue. *J Hazard Mater*. 2021;416:126124. <https://doi.org/10.1016/j.jhazmat.2021.126124>.
- Jenner LC, Rotchell JM, Bennett RT, Cowen M, Tentzeris V, Sadofsky LR. Detection of microplastics in human lung tissue using MFTIR spectroscopy. *Sci Total Environ*. 2022;831:154907. <https://doi.org/10.1016/j.scitotenv.2022.154907>.
- Wang M, Zhou T, Song Y, Li X, Ma H, Hu Y, et al. Joint exposure to various ambient air pollutants and incident heart failure: a prospective analysis in UK biobank. *Eur Heart J*. 2021;42 16:1582–91. <https://doi.org/10.1093/eurheartj/ehaa1031>.
- Jia Y, Lin Z, He Z, Li C, Zhang Y, Wang J, et al. Effect of air pollution on heart failure: systematic review and Meta-Analysis. *Environ Health Perspect*. 2023;131 7:76001. <https://doi.org/10.1289/ehp11506>.
- Yang Y, Xie E, Du Z, Peng Z, Han Z, Li L, et al. Detection of various microplastics in patients undergoing cardiac surgery. *Environ Sci Technol*. 2023;57 30:10911–8. <https://doi.org/10.1021/acs.est.2c07179>.
- Wang T, Yi Z, Liu X, Cai Y, Huang X, Fang J, et al. Multimodal detection and analysis of microplastics in human thrombi from multiple anatomically distinct sites. *EBioMedicine*. 2024;130:105118. <https://doi.org/10.1016/j.ebiom.2024.105118>.
- Guo X, Wang L, Wang X, Li D, Wang H, Xu H, et al. Discovery and analysis of microplastics in human bone marrow. *J Hazard Mater*. 2024;477:135266. <https://doi.org/10.1016/j.jhazmat.2024.135266>.
- Marfella R, Praticchizzo F, Sardu C, Fulgenzi G, Graciotti L, Spadoni T, et al. Microplastics and nanoplastics in atheromas and cardiovascular events. *N Engl J Med*. 2024;390 10:900–10. <https://doi.org/10.1056/NEJMoa2309822>.
- Zhang M, Shi J, Zhou J, Song L, Ding J, Deng HP, et al. N6-methyladenosine methylation mediates non-coding RNAs modification in microplastic-induced cardiac injury. *Ecotoxicol Environ Saf*. 2023;262:115174. <https://doi.org/10.1016/j.ecoenv.2023.115174>.
- Ye J, Qiu W, Pang X, Su Y, Zhang X, Huang J, et al. Polystyrene nanoplastics and cadmium co-exposure aggravated cardiomyocyte damage in mice by regulating PANoptosis pathway. *Environ Pollut*. 2024;347:123713. <https://doi.org/10.1016/j.envpol.2024.123713>.
- Zhang T, Yang S, Ge Y, Wan X, Zhu Y, Yang F, et al. Multi-dimensional evaluation of cardiotoxicity in mice following respiratory exposure to polystyrene nanoplastics. *Part Fibre Toxicol*. 2023;20(1):46. <https://doi.org/10.1186/s12989-023-00557-3>.
- Song Z, Wu H, Fang X, Feng X, Zhou L. The cardiovascular toxicity of polystyrene microplastics in rats: based on untargeted metabolomics analysis. *Front Pharmacol*. 2024;15:1336369. <https://doi.org/10.3389/fphar.2024.1336369>.
- Li Z, Zhu S, Liu Q, Wei J, Jin Y, Wang X, et al. Polystyrene microplastics cause cardiac fibrosis by activating Wnt/ β -catenin signaling pathway and promoting cardiomyocyte apoptosis in rats. *Environ Pollut*. 2020;265. <https://doi.org/10.1016/j.envpol.2020.115025>. Pt A:115025.
- Zhang Y, Yin K, Wang D, Wang Y, Lu H, Zhao H, et al. Polystyrene microplastics-induced cardiotoxicity in chickens via the ROS-driven NF- κ B-NLRP3-GSDMD and AMPK-PGC-1 α axes. *Sci Total Environ*. 2022;840:156727. <https://doi.org/10.1016/j.scitotenv.2022.156727>.
- Xiao Y, Hu L, Duan J, Che H, Wang W, Yuan Y, et al. Polystyrene microplastics enhance microcystin-LR-induced cardiovascular toxicity and oxidative stress in zebrafish embryos. *Environ Pollut*. 2024;352:124022. <https://doi.org/10.1016/j.envpol.2024.124022>.
- Zhang Y, Jiang Y, Zhu Z, Xu X, Yang H. Polyacrylonitrile microfibers pose a significant threat to the early-stage survival of zebrafish. *Aquat Toxicol*. 2023;265:106755. <https://doi.org/10.1016/j.aquatox.2023.106755>.
- Liu X, Liu Y, Chen X, Wang C, Chen X, Liu W, et al. Multi-walled carbon nanotubes exacerbate doxorubicin-induced cardiotoxicity by altering gut

- microbiota and pulmonary and colonic macrophage phenotype in mice. *Toxicology*. 2020;435:152410. <https://doi.org/10.1016/j.tox.2020.152410>.
24. Liu CX, Liu YB, Peng Y, Peng J, Ma QL. Causal effect of air pollution on the risk of cardiovascular and metabolic diseases and potential mediation by gut microbiota. *Sci Total Environ*. 2024;912:169418. <https://doi.org/10.1016/j.scitotenv.2023.169418>.
 25. Flint HJ, Scott KP, Louis P, Duncan SH. The role of the gut microbiota in nutrition and health. *Nat Rev Gastroenterol Hepatol*. 2012;9 10:577–89. <https://doi.org/10.1038/nrgastro.2012.156>.
 26. Witkowski M, Weeks TL, Hazen SL. Gut microbiota and cardiovascular disease. *Circ Res*. 2020;127 4:553–70. <https://doi.org/10.1161/circresaha.120.316242>.
 27. Haghikia A, Zimmermann F, Schumann P, Jasina A, Roessler J, Schmidt D, et al. Propionate attenuates atherosclerosis by immune-dependent regulation of intestinal cholesterol metabolism. *Eur Heart J*. 2022;43 6:518–33. <https://doi.org/10.1093/eurheartj/ehab644>.
 28. Tang WH, Hazen SL. Microbiome, trimethylamine N-oxide, and cardiometabolic disease. *Transl Res*. 2017;179:108–15. <https://doi.org/10.1016/j.trsl.2016.07.007>.
 29. Zhang Z, Lv T, Wang X, Wu M, Zhang R, Yang X, et al. Role of the microbiota-gut-heart axis between bile acids and cardiovascular disease. *Biomed Pharmacother*. 2024;174:116567. <https://doi.org/10.1016/j.biopha.2024.116567>.
 30. Jonsson AL, Bäckhed F. Role of gut microbiota in atherosclerosis. *Nat Rev Cardiol*. 2017;14 2:79–87. <https://doi.org/10.1038/nrcardio.2016.183>.
 31. Kang H, Zhang W, Jing J, Huang D, Zhang L, Wang J, et al. The gut-brain axis involved in polystyrene nanoplastics-induced neurotoxicity via reprogramming the circadian rhythm-related pathways. *J Hazard Mater*. 2023;458:131949. <https://doi.org/10.1016/j.jhazmat.2023.131949>.
 32. Zhang Z, Xu M, Wang L, Gu W, Li X, Han Z, et al. Continuous oral exposure to micro- and nanoplastics induced gut microbiota dysbiosis, intestinal barrier and immune dysfunction in adult mice. *Environ Int*. 2023;182:108353. <https://doi.org/10.1016/j.envint.2023.108353>.
 33. Chen HC, Liu YW, Chang KC, Wu YW, Chen YM, Chao YK, et al. Gut butyrate-producers confer post-infarction cardiac protection. *Nat Commun*. 2023;14(1):7249. <https://doi.org/10.1038/s41467-023-43167-5>.
 34. Hu T, Wu Q, Yao Q, Jiang K, Yu J, Tang Q. Short-chain fatty acid metabolism and multiple effects on cardiovascular diseases. *Ageing Res Rev*. 2022;81:101706. <https://doi.org/10.1016/j.arr.2022.101706>.
 35. Hunter RW, Hughey CC, Lantier L, Sundelin EI, Peggie M, Zeqiraj E, et al. Metformin reduces liver glucose production by inhibition of fructose-1-6-bisphosphatase. *Nat Med*. 2018;24 9:1395–406. <https://doi.org/10.1038/s41591-018-0159-7>.
 36. Choi JW, Jo SW, Kim DE, Paik IY, Balakrishnan R. Aerobic exercise attenuates LPS-induced cognitive dysfunction by reducing oxidative stress, glial activation, and neuroinflammation. *Redox Biol*. 2024;71:103101. <https://doi.org/10.1016/j.redox.2024.103101>.
 37. Hua J, Zhang T, Chen X, Zhu B, Zhao M, Fu K, et al. Behavioral impairments and disrupted mitochondrial energy metabolism induced by polypropylene microplastics in zebrafish larvae. *Sci Total Environ*. 2024;947:174541. <https://doi.org/10.1016/j.scitotenv.2024.174541>.
 38. Dimitriadi A, Papaefthimiou C, Genizegkini E, Sampsonidis I, Kalogiannis S, Feidantsis K, et al. Adverse effects polystyrene microplastics exert on zebrafish heart-Molecular to individual level. *J Hazard Mater*. 2021;416:125969. <https://doi.org/10.1016/j.jhazmat.2021.125969>.
 39. Lin P, Tong X, Xue F, Qianru C, Xinyu T, Zhe L et al. Polystyrene nanoplastics exacerbate lipopolysaccharide-induced myocardial fibrosis and autophagy in mice via ROS/TGF- β 1/Smad. *Toxicology*. 2022;480:153338. <https://doi.org/10.1016/j.tox.2022.153338>.
 40. Zhou Y, Wu Q, Li Y, Feng Y, Wang Y, Cheng W. Low-dose of polystyrene microplastics induce cardiotoxicity in mice and human-originated cardiac organoids. *Environ Int*. 2023;179:108171. <https://doi.org/10.1016/j.envint.2023.108171>.
 41. Zmora N, Suez J, Elinav E. You are what you eat: diet, health and the gut microbiota. *Nat Rev Gastroenterol Hepatol*. 2019;16 1:35–56. <https://doi.org/10.1038/s41575-018-0061-2>.
 42. Krautkramer KA, Fan J, Bäckhed F. Gut microbial metabolites as multi-kingdom intermediates. *Nat Rev Microbiol*. 2021;19 2:77–94. <https://doi.org/10.1038/s41579-020-0438-4>.
 43. Zhang D, Jian YP, Zhang YN, Li Y, Gu LT, Sun HH, et al. Short-chain fatty acids in diseases. *Cell Commun Signal*. 2023;21 1:212. <https://doi.org/10.1186/s12964-023-01219-9>.
 44. Poll BG, Cheema MU, Pluznick JL. Gut microbial metabolites and blood pressure regulation: focus on SCFAs and TMAO. *Physiology*. 2020;35 4:275–84. <https://doi.org/10.1152/physiol.00004.2020>.
 45. Jin Y, Wu S, Zeng Z, Fu Z. Effects of environmental pollutants on gut microbiota. *Environ Pollut*. 2017;222:1–9. <https://doi.org/10.1016/j.envpol.2016.11.045>.
 46. Ran Z, An Y, Zhou J, Yang J, Zhang Y, Yang J, et al. Subchronic exposure to concentrated ambient PM_{2.5} perturbs gut and lung microbiota as well as metabolic profiles in mice. *Environ Pollut*. 2021;272:115987. <https://doi.org/10.1016/j.envpol.2020.115987>.
 47. Park SK, Kang JY, Kim JM, Kim MJ, Lee HL, Moon JH, et al. *Porphyra tenera* protects against PM_{2.5}-Induced cognitive dysfunction with the regulation of gut function. *Mar Drugs*. 2022;20:7. <https://doi.org/10.3390/md20070439>.
 48. Jalali S, Karbakhsh M, Momeni M, Taheri M, Amini S, Mansourian M, et al. Long-term exposure to PM_{2.5} and cardiovascular disease incidence and mortality in an Eastern mediterranean country: findings based on a 15-year cohort study. *Environ Health*. 2021;20(1):112. <https://doi.org/10.1186/s12940-021-00797-w>.
 49. Bartolomeaus H, Balogh A, Yakoub M, Homann S, Markó L, Höges S, et al. Short-Chain fatty acid propionate protects from hypertensive cardiovascular damage. *Circulation*. 2019;139 11:1407–21. <https://doi.org/10.1161/circulationaha.118.036652>.
 50. De Vadder F, Kovatcheva-Datchary P, Goncalves D, Vinera J, Zitoun C, Duchamp A, et al. Microbiota-generated metabolites promote metabolic benefits via gut-brain neural circuits. *Cell*. 2014;156(1–2):84–96. <https://doi.org/10.1016/j.cell.2013.12.016>.
 51. Kang H, Huang D, Zhang W, Wang J, Liu Z, Wang Z, et al. Inhaled polystyrene microplastics impaired lung function through pulmonary flora/TLR4-mediated iron homeostasis imbalance. *Sci Total Environ*. 2024;946:174300. <https://doi.org/10.1016/j.scitotenv.2024.174300>.
 52. Wu Z, He J, Zhang Z, Li J, Zou H, Tan X, et al. Propionic acid driven by the *Lactobacillus johnsonii* culture supernatant alleviates colitis by inhibiting M1 macrophage polarization by modulating the MAPK pathway in mice. *J Agric Food Chem*. 2023;71 41:14951–66. <https://doi.org/10.1021/acs.jafc.3c00278>.
 53. Lin ZH, Li YC, Wu SJ, Zheng C, Lin YZ, Lian H, et al. Eliciting α -7nAChR exerts cardioprotective effects on ischemic cardiomyopathy via activation of AMPK signalling. *J Cell Mol Med*. 2019;23 7:4746–58. <https://doi.org/10.1111/jcmm.14363>.
 54. Villavicencio C, Daniel X, Cartanyá M, Leache J, Ferré C, Roure M, et al. Cardiac output in critically ill patients can be estimated easily and accurately using the minute distance obtained by pulsed-wave doppler. *Shock*. 2023;60 4:553–9. <https://doi.org/10.1097/shk.0000000000002210>.
 55. Sattin M, Burhani Z, Jaidka A, Millington SJ, Arntfield RT. Stroke volume determination by echocardiography. *Chest*. 2022;161 6:1598–605. <https://doi.org/10.1016/j.chest.2022.01.022>.
 56. Kennel PJ, Mancini DM, Schulze PC. Skeletal muscle changes in chronic cardiac disease and failure. *Compr Physiol*. 2015;5 4:1947–69. <https://doi.org/10.1002/cphy.c110003>.
 57. Lokugamage MP, Vanover D, Beyersdorf J, Hatit MZC, Rotolo L, Echeverri ES, et al. Optimization of lipid nanoparticles for the delivery of nebulized therapeutic mRNA to the lungs. *Nat Biomed Eng*. 2021;5 9:1059–68. <https://doi.org/10.1038/s41551-021-00786-x>.
 58. Jing J, Zhang L, Han L, Wang J, Zhang W, Liu Z, et al. Polystyrene micro-/nanoplastics induced hematopoietic damages via the crosstalk of gut microbiota, metabolites, and cytokines. *Environ Int*. 2022;161:107131. <https://doi.org/10.1016/j.envint.2022.107131>.
 59. Kang H, Huang D, Zhang W, Wang J, Liu Z, Wang Z, et al. Pulmonary flora-derived lipopolysaccharide mediates lung-brain axis through activating microglia involved in polystyrene microplastic-induced cognitive dysfunction. *Adv Sci*. 2024;11:e2404966. <https://doi.org/10.1002/adv.202404966>.

Publisher's note

Springer Nature remains neutral with regard to jurisdictional claims in published maps and institutional affiliations.